SANS investigation of the salt-crystallization- and surface-treatment-induced degradation on limestones of historic–artistic interest

Cettina Bottari[1] · Gino Mirocle Crisci[2] · Vincenza Crupi[1] · Valeria Ignazzitto[1] ·
Mauro Francesco La Russa[2] · Domenico Majolino[1] · Michela Ricca[2] ·
Barbara Rossi[3] · Silvestro Antonio Ruffolo[2] · Josè Teixeira[4] · Valentina Venuti[1]

Abstract We present here a small-angle neutron scattering investigation on typical limestone widely used in the Baroque architecture of Modica (eastern Sicily). The aim was to correlate the salt weathering and, after that, consolidating (using nanolime as consolidant product) behaviour of the mesoscopic features observed in the experiment, with particular regard to the pore structure, which determines the interaction between surface and environmental/consolidating agents. Experimental results have been interpreted in terms of a fractal model that revealed successful in characterizing physical properties induced by treatment, in order to predict the behaviour of consolidated stone against salt weathering.

1 Introduction

The world's artistic and cultural heritage is constantly exposed to degradation processes, induced by both natural and human effects that cause alterations of the structure of the stone material by increasing the distribution of the pores and reducing the compactness and therefore the durability of the architectural work. Nowadays, one of the most serious problems facing conservation is represented by deterioration of stone materials used in works of artistic/architectural interest, such as lime-based wall paintings, calcareous stones, marbles, ceramics and pottery. Air pollution, soluble salts and bio-deterioration are the main causes of decay, and the existing literature includes many papers concerning the investigation of their mechanisms of action [1, 2]. The preservation of stone buildings of historic–artistic interest is a multi-disciplinary task that requires a broad knowledge of the porous structure of materials and the effects that the external environment generates on them [3]. As a matter of fact, only after a full understanding of the characteristics of these materials and their behaviour during the degradation process, it will be, in principle, possible to apply the appropriate operations that involve not only restoration, handling and conservation, but also prevention and control [4, 5].

Water can be retained one of the main causes of deterioration, since, migrating through the porous stone material and evaporating within the pores, it leaves extremely harmful salt deposits. The salts crystallization within the porous structure gives rise to a pressure increasing that originates a mechanical effect on the surface of the pore itself, resulting in a worsening of the chemical–physical properties of the material in the form of microcracks, delamination of fragments and complete disintegration of the material itself [6, 7]. Again, the environmental conditions, responsible for the temperature changes, can cause changes in the volume of the saline solution in the transition from liquid to solid state, resulting in a loss of cohesion of the rock material. Known since ancient times the degrading effect of water, great attention has always been paid in the research of protective and/or consolidating

✉ Valentina Venuti
  vvenuti@unime.it

1 Dipartimento di Scienze Matematiche Informatiche, Scienze Fisiche e Scienze della Terra, Università di Messina, Viale Ferdinando Stagno D'Alcontres 31, 98166 Messina, Italy

2 Dipartimento di Biologia, Ecologia e Scienze della Terra (DiBEST), Università della Calabria, Via Pietro Bucci, Arcavacata di Rende, 87036 Cosenza, Italy

3 Elettra-Sincrotrone Trieste, Strada Statale 14 km 163.5, Area Science 70 Park, 34149 Basovizza, Trieste, Italy

4 Laboratoire Léon Brillouin, CEA Saclay, 91191 Gif-sur-Yvette Cedex, France

agents, aimed at limiting the absorption of the fluid in the porous medium.

In the last years, colloid and material sciences revealed effective tools in the field of cultural heritage conservation, increasing the performance of products and minimizing drawbacks and negative effects [8]. In particular, it has been proven that the use of nanoparticles in the field of conservation allows to enhance the performance of treatments [9, 10].

Recently [11], we assessed the salt weathering behaviour of Modica limestones, largely used in the Baroque architecture of the cities of Modica and Ragusa (Eastern Sicily, Italy), included in the UNESCO's World Heritage List since 2002. Then, degraded samples were treated with different consolidating products, and peeling tests, point load tests and mercury intrusion porosimetry (MIP) were used to investigate the changes induced by treatment in the pore structure, the correlation between salt crystallization and microstructural features of the limestone, as well as the efficacy of treatments. Furthermore, treated samples were weathered in order to assess their behaviour against further salt crystallization processes. From the results, nanolime is shown to provide a good mechanical strength to degraded stone and a good resistance against salt weathering.

Based on the aforementioned results, the present work is aimed at the quantitative investigation, in a microdestructive way, by means of small-angle neutron scattering (SANS) technique, of the porous structure evolution in Modica limestones, during salt crystallization process and as a consequence of treatment with a consolidating agent, i.e. a suspension of nanolime in alcohol. As well known, the pressure of crystallization that the salt exerts on pore walls is strictly dependent on the porous structure. Then, the mesoscopic structural parameters as obtained from SANS [12] are crucial to get information concerning the damage produced by the development of fractures and disaggregation due to the salt crystallization in the limestones. Again, SANS analysis can furnish useful information regarding the effect of the surface treatment with specific products that, being deposited on the surface, will change the surface properties of the stone.

The use of SANS for the investigation of porosity at nanoscale level, in conjunction with the already performed routine determination of porosity at sub-micrometric dimensional scale by usual filling methods such as MIP, revealed appropriate because of the variability of the size distribution [13–15].

In this sense, SANS analysis, covering the lack of information on small pores (<10 nm), made possible to assess with a better accuracy the crystallization pressures process and the micro–nanostructural variations. Other than the wide extension of the explored spatial range offered by SANS with respect to MIP, a quite new aspect of the present approach is given by the fact that in the SANS experiment,

the average radius of the pores is obtained by using an approach introduced at the end of nineties, involving the concept of fractal surface by a direct evaluation of the total surface area of the solid/air interface [16]. Furthermore, in this topic, the effects of degradation process are frequently limited to a qualitative description, while there are only a few examples of studies on which quantitative view, as the one investigated here, is obtained [4].

Finally, the SANS technique could be very useful in detailed studies of particle pore distributions, which are particularly relevant for testing a new consolidating agent; in such cases, it is worth checking the satisfactory behaviour of the treatment in advance.

2 Materials and methods

2.1 Samples

Limestones analysed in this experimental study come from a historical quarry located in Modica, in the province of Ragusa (Eastern Sicily, Italy). This stone is largely used in the monuments of the Baroque cities of Ragusa and Modica [17, 18], included in the UNESCO's World Heritage List since 2002.

From a macroscopic point of view, the Modica stone samples are characterized by white–cream colour, homogeneous texture and medium-fine grain size. Petrographic observations [18] revealed a grain-supported texture with about 30 % of micritic matrix. Allochemical components, with percentages between 40 and 45 %, consist of several bioclasts, mainly made by fragments of echinoderms, peloids, foraminifera, scaphopoda worms and shellfish. Intergranular spaces are filled with micrite, locally neomorphosed to microsparite. The porosity (about 27 %) is mainly intergranular. According to Dunham [19], Modica stone can be classified as a packstone.

The salt crystallization test (or salt weathering test), was performed on cubic specimens (5 cm). The procedure followed for salt crystallization is that described in the existing standard [20] Specifically, specimens (size $5 \times 5 \times 5$ cm) underwent several crystallization cycles (1, 6, 15) consisting of: 2 h of immersion in a supersaturated solution of sodium sulphate (14 % w/w at 20 °C), 16 h of drying in an oven at 105 °C and 6 h of cooling at room temperature. The weight of each test sample was measured before the crystallization test, and after each cycle, the resulting weight loss was determined. Real deterioration phenomenology, which occurs outdoor and involves many parameters, can deviate from those induced in laboratory; however, the adoption of a standardized method represents the only way to assure a certain repeatability and reproducibility of the experiment.

Before consolidation, desalinization of weathered samples has been performed through immersion in distilled water for 24 h, and after this, water was discarded and the process was repeated with new distilled water. The procedure was stopped as the water conductivity reached a constant value. This procedure, if applicable, represents a desirable process in restoration works, in order to remove salts from the stone, since they can be highly dangerous once entrapped in the porous structure after a consolidation treatment. The desalinization method used in this paper is quite different from those procedures adopted in situ by restorers, the latter can in fact lead to highly variable effects, while our desalinization method provides more reliable results.

For the stone consolidation treatment, we used nanolime (nLime) (Nano Restore, CTS, Italy), a suspension of nano-sized lime ($CaOH_2$) in isopropyl alcohol having a concentration of 5 % m/m. This product, despite having a great potential for the restoration of cultural heritage, has to be better explored, in terms of efficacy on a variety of materials, as well as in terms of long-term behaviour. These are probably the main reasons for its limited use, at least up to now. Specimens have been immersed in the suspension for 15 days, and then, samples were allowed to dry at room temperature (25 °C). Measurements have been performed after a month, when a constant value in the sample mass was achieved.

The experimentation consisted of two steps: (1) salt weathering of untreated samples (Fig. 1) and (2) stone consolidation. It is aimed at understanding the behaviour of consolidation treatment in different situations: slightly, moderately and highly degraded material.

Table 1 reports the sample list. It is worth remarking that, for each sample group, different sections have been analysed, so the reported SANS spectra are averaged for the different sections of each group.
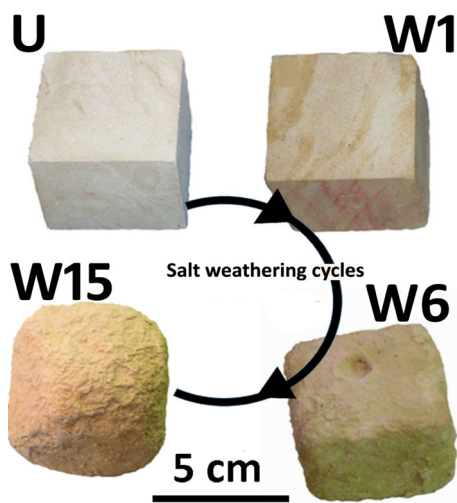

Fig. 1 Unweathered and weathered Modica stone specimens

Table 1 List of analysed samples and details on the experimentation

Sample group	Step 1, salt weathering (number of cycles)	Step 2, desalinization + consolidation	Number of samples
U	–	–	3
W1	1	–	4
W6	6	–	2
W15	15	–	2
W1-nLime	1	nLime	3
W6-nLime	6	nLime	3
W15-nLime	15	nLime	2

2.2 Small-angle neutron scattering (SANS) measurements

The aim of a SANS experiment is to obtain structural information about inhomogeneity in materials with a characteristic size approximately ten to hundreds of angstroms [21]. SANS allows determining shape and organization, averaged in time, of particles or aggregates dispersed in a continuous medium.

In a SANS experiment, a beam of collimated neutrons of wavelength hits a sample, illuminating a volume V, which can be an aqueous solution, a solid, a powder or a crystal. The scattering centres (nuclei) of the sample form a grating (space lattice) of periodicity equal to the average atomic distance, d, which deflects the neutron trajectories. In an ideal case, the neutron beam can be viewed as an assembly of particles flying in parallel directions at the same speed. It can be described by a planar monochromatic wave having a propagation equation that can be written as

$$\varphi(x,t) = \varphi_0 e^{-i(k_i x - \omega t)}, \qquad (1)$$

where $2\pi/T$ is the pulsation and $\vec{k}_i$ is the incident wavevector. Some of the incident radiation is transmitted by the sample, some absorbed and some scattered. In SANS, only the coherent elastic interaction between the neutron beam and the sample is considered. In an elastic scattering event, the scattered particle does not exchange energy with the scattering medium so that its wavelength remains unaltered, only the wavevector changes direction. The exchanged momentum indicates the difference between incident and scattered wavevectors, and its modulus is expressed by

$$\left|\vec{Q}\right| = \left|\vec{k}_f - \vec{k}_i\right| = \frac{4\pi}{\lambda}\sin\frac{\theta}{2} \qquad (2)$$

where θ is the angle between $\vec{k}_f$ and $\vec{k}_i$. Combining the latter equation with Bragg law, one obtains $\left|\vec{Q}\right| = 2\pi/d$, being d the interlayer spacing between two layers in a crystal lattice. Hence, for investigating large-scale structures, very

small Q values are necessary, whereas large Q values allow exploring small scattering centres or distances.

The objective of a SANS experiment is to determine the scattering intensity versus exchanged momentum, $I(Q)$, which is a picture in the reciprocal space of mesoscopic features of sizes between 10 and 104 Å, so providing information on the shape, size and interactions of the scattering bodies (assemblies of scattering centres) in the sample. It is generally expressed [12, 21] as follows:

$$I(Q) = \Phi P(Q)\overline{S}(Q) \tag{3}$$

In this expression, $\Phi = N/V$ is the number density, expressed in cm^{-3}, where N is the number of scattering centres and V is the volume of the sample.

Again, $P(Q)$ is defined as:

$$P(Q) = \left\langle |F(Q)|^2 \right\rangle = \left\langle \left| \int_V [\rho(\vec{r}) - \rho_0] \exp\left(i\vec{Q} \cdot \vec{r}\right) d\vec{r} \right|^2 \right\rangle, \tag{4}$$

in which $\rho(\vec{r})$ and ρ_0 are the coherent scattering length density of the scatterers and of the continuous medium, respectively. Their difference $K = \rho(\vec{r}) - \rho_0$ is named contrast. The Fourier transform of the contrast evaluated over the volume of the particle is the form factor $F(Q)$. $P(Q)$, the square of the modulus of $F(Q)$ averaged over the ensemble of particles, depends on the geometrical form and dimension of the mesoscopic units within the sample.

For diluted particles, the value of $P(Q)$ in the range where $QR \ll 1$, if R is the particle radius, is given by [22]

$$P(Q) = K^2 V^2 \exp\left(-Q^2 R_g^2/3\right), \tag{5}$$

in which R_g is the radius of gyration of the particle and V its volume.

At large values of Q, the scattered intensity becomes independent on the shape of the particle and is dominated by surface scattering. In this domain, $P(Q)$ is given by the Porod equation:

$$P(Q) = 2\pi K^2 S Q^{-4} \tag{6}$$

where S is the total area of the surface.

Finally, $\overline{S}(Q)$ is the interparticle term, an effective structure factor defined by:

$$\overline{S}(Q) = 1 + \frac{|\langle F(Q) \rangle|^2}{\langle |F(Q)|^2 \rangle}[S(Q) - 1]. \tag{7}$$

In the above expression, the structure factor $S(Q)$ is related to the Fourier transform of the pair correlation function $g(r)$ by:

$$S(Q) = 1 + \Phi \int [g(r) - 1] \exp\left(i\vec{Q} \cdot \vec{r}\right) d\vec{r}, \tag{8}$$

where $\Phi g(r)$ indicates the probability of finding a particle at a distance r from a particle situated at the origin.

As a matter of fact, $S(Q)$ describes how $I(Q)$ is modulated by interference effects between radiation scattered by different scattering bodies.

Starting from the late 1980s, SANS technique has been widely used in petrography to demonstrate the fractal character of rocks, determining their fractal dimension [23].

Fractals are characterized by self-similarity within some spatial range, i.e. the structure is independent on the length scale of observation in that range. If one measures the mass M of a material in a volume r^d, it is related to that length scale by $M(r) \sim r^D$, where D is the fractal dimension, smaller than the dimension d of the space. The density of the sample varies as ρr^{D-d}, and by Fourier transform, one obtains the scattering law

$$I(Q) \approx Q^{-D}. \tag{9}$$

For fractal surfaces characterized by a surface fractal dimension D_s ($2 \leq D_s \leq 3$), the scattering law becomes

$$I(Q) \approx Q^{-(6-D_s)}. \tag{10}$$

The above relations are valid for ideal fractals throughout the Q range, whereas, for real fractals, they are applicable only over a limited Q range, $\xi^{-1} < Q < r_0^{-1}$, where r_0 is the size of single particles in an aggregation process, and ξ the size of the aggregates.

SANS measurements were performed on the PAXY spectrometer at the ORPHEE reactor of the Laboratoire Léon Brillouin (LLB, Saclay, France) [24]. Two configurations have been used: large Q with $\lambda = 5$ Å, sample-detector distance = 5 m and Q range extending from 1.3×10^{-2} to 9.8×10^{-2} Å^{-1}; and small Q with $\lambda = 16$ Å, sample-detector distance = 5 m and Q range extending from 3.9×10^{-3} to 3×10^{-2} Å^{-1}.

Measured samples were cut in thin sections (thickness <1 mm), in order to minimize problems arising from multiple scattering effects. It is worth remarking that even if SANS is a useful technique for nondestructive measurement, in this case, we are operating in microdestructive conditions. No appreciable neutron activation of the samples was found after the experiment. By the standard LLB SANS routines, the two-dimensional intensity distributions were corrected for background and normalized to absolute intensity by measuring incident beam intensity, transmission and thickness of each sample. By integrating the normalized two-dimensional intensity distribution with respect to the azimuthal angle, we obtained one-dimensional scattering intensity distributions $I(Q)$ expressed as the unit differential cross section per unit volume of the sample (cm^{-1}). The obtained results have been compared to those obtained from mercury intrusion porosimetry

(MIP) analysis, which consists in the progressive intrusion of mercury into a porous structure under controlled pressures. From the pressure versus intrusion data, it is possible to calculate volume and size distributions of pores, the higher is the pressure the smaller are the pores. Moreover, it is possible to calculate the backbone and the percolation fractal dimensions [25], D_B and D_P, respectively, the first one is related to the larger pores, while the second is calculated from the smaller ones.

3 Results and discussion

One of the main difficulties encountered in the interpretation of SANS data from natural stones with organic content derives from the multiphase character of the scattering medium, that contains, other than specific lithological components, entrapped water and gas (or even voids spaces). However, for the purposes of the study of the surface roughness and porosity, the systems can be considered as composed of grains, water and/or voids [26]. Treated samples are assumed as the same as untreated ones, since nanolime, once reacted, turns into calcite, which has similar composition and can be assumed having similar morphology in comparison with the stone. Weathered stone contains a certain amount of residual sodium sulphate; however, even in this case, the system is simplified as for untreated specimens.

Figure 2 reports, in a log–log plot, the evolution of the SANS profiles upon degradation induced by salt crystallization (Fig. 2a) or by consolidation (Fig. 2b).

From a first inspection of the figures, it seems that the main differences in the experimental profiles can be observed in the low-Q region of the spectra that, as described in Sect. 2, gives information of the radius of gyration R_g of the mesoscopic units. In the high-Q region, the linear behaviour of $I(Q)$ testifies the fractal nature of the interfaces between grains in the sample. In this range, the slope of the curves, associated with the surface fractal dimension, look almost similar.

Now, making reference to an empirical approach [27], already successfully applied for a variety of stones of historical–artistic interest [13–15, 28, 29], the description of SANS spectra has been performed hypothesizing the existence, for our investigated limestones, of two independent populations, associated with mesoscopic units with different dimensions and geometries. On one side, "small" units, i.e. new formation mineral clusters or crystallites, are accessible in the investigated Q range, on the other side, "big" units, i.e. voids or mineral aggregates, have typical size out of the experimental spatial window, and hence, only their surface can be probed.
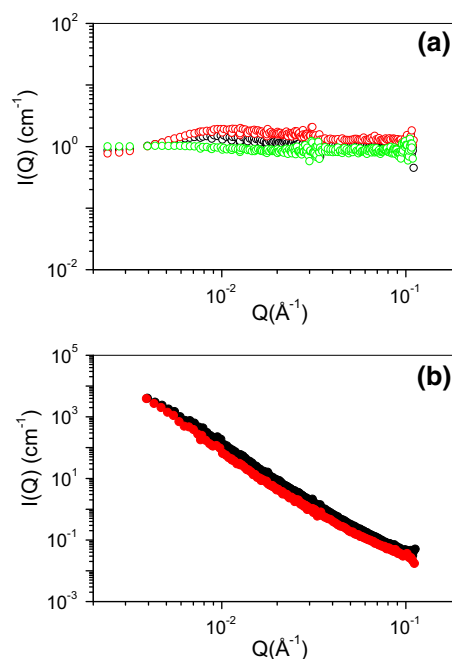

Fig. 2 a Experimental SANS spectra of Modica stones weathered by 1, 6, 15 salt crystallization cycles (W1, W6 and W15 specimens, *black*, *red* and *green open circles*, respectively). The spectra are normalized with respect to untreated U specimen. *Error bars* within symbols. **b** Experimental SANS spectra of Modica stone weathered by 6 salt crystallization cycles (W6 specimen, *black closed circles*) and, after that, treated with Nanorestore® (W6-nLime specimen, *red closed circles*). *Error bars* within symbols

Because of the substantially different dimensions of the corresponding structures, these two populations will independently contribute to the scattering, and hence, the resulting fitting law will be the weighted sum of a Guinier law ascribed to "small" units, and a power law associated to "big" units, plus a low-level scattering background B representing the contribution of incoherent scattering of hydrogen atoms:

$$I(Q) \cong C_1 \exp\left(\frac{-Q^2 R_g^2}{3}\right) + C_2 Q^{-\alpha} + B. \quad (11)$$

In the above expression, the prefactors C_1 and C_2 contain the relative intensity of the Guinier and power laws. The radius of gyration R_g provides the mean size of newly formed mineral clusters or crystallites, whereas the exponent α is related to the surface fractal dimension D_s by $\alpha = 6 - D_s$ and accounts for the roughness of the voids or mineral aggregates. According to the fractal model, $2 \leq D_s \leq 3$, so implying $3 \leq \alpha \leq 4$. The two-dimensional Euclidean exponent $D_s = 2$ (and hence $\alpha = 4$) is restored for particles with sharp interfaces.

Figure 3 depicts the best-fit results as obtained for samples U, W15, and W15-nLime, as examples.
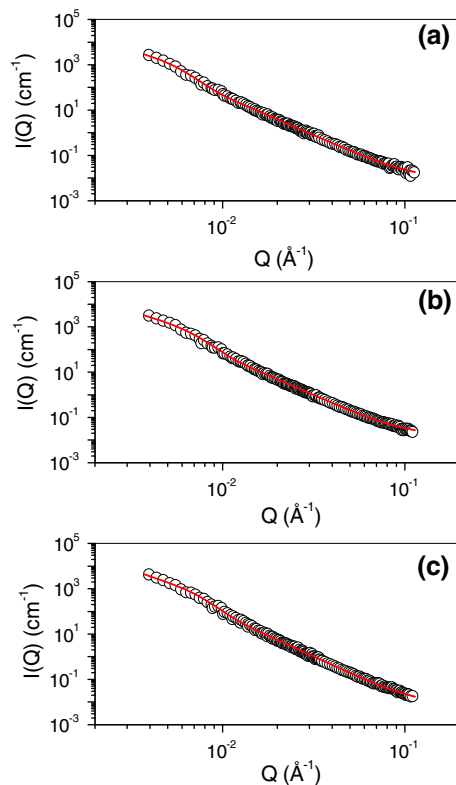
Fig. 3 Experimental SANS spectra (*black open circles*) of U (**a**), W15 (**b**) and W15-nLime (**c**) samples, together with the best-fit (*red line*) according to Eq. (11). *Error bars* within symbols

For all the analysed samples, the extracted values of R_g, α and D_s are reported in Table 2.

Firstly, we observe that the value of the fractal exponent α turns out always between 3 and 4. This indicates that the fractal surface model applies well to all the analysed samples and suggests that structural rearrangements reactions occur with the development of "viscous finger" interfaces with fractal geometry, in agreement with what

Table 2 Radius of gyration R_g, fractal exponent α and surface fractal dimension D_s for all the investigated samples (see text for details)

Sample	R_g [Å]	α	D_s
U	453.5	3.49	2.51
W1	304.1	3.53	2.47
W6	321.9	3.57	2.43
W15	401.6	3.69	2.31
W1-nLime	307.4	3.40	2.60
W6-nLime	396.9	3.56	2.44
W15-nLime	406.6	3.67	2.33

Error bars for R_g are, on average, of the order of 7 % (4 and 10 % for the lower and higher values, respectively). Error bars for α and D_s are of the order of 1 %. The quality of the fitting is testified by Chi-square ~ 0.9999

already observed in a variety of stones of different type [4, 13–15, 27].

Weathering is shown to cause an initial falling down of R_g with respect to untreated sample, whose highest value of R_g suggests a sub-micrometric granulometry of the mesoscopic structure. After that, a progressive enhancement is revealed when the number of cycles of salt crystallization increases. This trend is indicative of an initial structural rearrangement, followed by a growing of the corresponding mesoscopic aggregates.

The degradation associated with an increasing of the number of cycles of salt crystallization causes an enhancement of the sharpness of the interfaces, as expressed by the increased value of α. This result, in agreement with a previous neutron radiography study on the deterioration processes in limestones [30], can be justified thinking that salt crystallization can generate cracks within the material that, in turn, can generate new pores and also connections between blind pores and open pores structure [6].

Passing from the weathered samples to the corresponding treated ones, one can observe that treatment with nanolime contributes to slightly enlarge the size of the "small" units and induces, at the same time, an increasing of the value of D_S associated to the "big" aggregates. These occurrences can be explained in terms of a chemical affinity of nanolime for specific sites on the interfaces, and testify the efficacy of the treatment.

Again, the low-level scattering background B obtained by the fitting procedure, representing the incoherent scattering contribution due to hydrogen atoms, allows an estimation of the number N_H of hydrogen atoms per unit volume of the sample, by using:

$$N_H = \frac{B}{\frac{\sigma_{inc}}{4\pi}} = \left(\frac{\pi}{20}\right) \times 10^{24} B \qquad (12)$$

in which $\sigma_{inc} = 80 \times 10^{-24}$ cm^2 represents the incoherent cross section of hydrogen. B and N_H values are reported in Table 3 for all the analysed samples.

Table 3 Low-level scattering background B and corresponding number N_H of hydrogen atoms per unit volume for all the investigated samples

Sample	B (cm^{-1})	N_H (10^{21} cm^{-3})
U	0.012	1.88
W1	0.019	2.98
W6	0.015	2.36
W15	0.015	2.35
W1-nLime	0.008	1.26
W6-nLime	0.014	2.20
W15-nLime	0.009	1.41

For all samples, hydrogen atoms are those of water molecules adsorbed in pores or located at the interfaces. Their number per unit volume of the sample will be given by $N_{H_2O} = N_H/2 = 0.94 \times 10^{21}$ cm^{-3}.

Weathered samples show higher values of N_H with respect to untreated and consolidated stone. This can be due to the higher affinity of the residual salts within the porous structure; indeed, sodium sulphate has a strong hygroscopic feature. The consolidation of weathered samples has been carried out once desalinization, so there is not any salt crystals left into the stone.

In addition, mercury intrusion porosimetry (MIP) measurements were already performed on these samples [9], and the data have been now processed taking into account the method proposed by Angulo et al. [25], in order to extract information about the fractal characteristics of the pore space of the sample material. In our case, linear regions in the log–log plot of intrusion volume versus pressure have been recognized, implying that pore volume has fractal dimensions. The value of the fractal dimension of the material in the linear range is extracted from the inverse log of the equation. In particular, the presence of two regions of linearity is found in the data from the investigated materials; this is attributed to there being two different processes related to pore space. The lower pressure linear region occurs during "backbone formation" (larger pores) when mercury is finding a conductivity path through the pore structure. The adjacent linear region at higher pressure occurs during "percolation" (exploring smaller pores) where flow through the medium is optimized. From them, we obtained, the backbone fractal dimension D_B and the percolation fractal dimension D_P, respectively. The backbone fractal dimension D_B is calculated from large pore size exploration, while the percolation fractal dimension D_P is related to the small pores. Their values are reported in Table 4.

Regarding the fractal dimensions calculated from MIP measurements, it is worth to note that the percolation fractal dimension D_P is quite insensitive to the degradation process, as well as to the consolidation procedure. On the contrary, the backbone fractal dimension D_B has similar trends to D_S extracted by SANS.

3.1 Determination of the total surface of the interfaces and other relevant aspects

In the framework of the fractal model, a comparison, in the high-Q range, of the linear fit for the scattered intensity $I(Q)$, given by $C_2 Q^{-\alpha}$, with the Porod's law $I(Q) = 2\pi K^2 S Q^{-4}$ allows an estimation of the total surface S of the interfaces per unit volume of the sample. It is worth remarking that all interfaces are "seen" by the neutron probe, included closed pores. In the above expression, the contrast K^2 was calculated from an average density weighted by the fraction resulting in the quantitative chemical composition previously determined by XRF measurements not reported here.

Specifically, chosen two different Q values within the fractal domain, namely $Q_1 = 0.04$ Å^{-1} and $Q_2 = 0.1$ Å^{-1}, the comparison gives $C_2 Q_1^{-\alpha} = 2\pi K^2 S_{Q_1} Q_1^{-4}$ and $C_2 Q_2^{-\alpha} = 2\pi K^2 S_{Q_2} Q_2^{-4}$ for Q_1 and Q_2, respectively. S_{Q_1} and S_{Q_2} are measures of the same interface area evaluated at a scale $1/Q_1$ and $1/Q_2$, respectively.

Table 5 reports the obtained C_2, K^2, S_{Q_1} and S_{Q_2} values.

In Table 5, we also report the evaluated number of hydrogen atoms per unit interface area, N_H/S_{Q_2}. For this calculation, the use of S_{Q_2}, corresponding to a uniform coverage of the interfaces with molecules of sizes $1/Q_2$, appeared more appropriate, considering the size of the molecules of the adsorbed layer. For all the investigated samples, this value turned out to be almost equal to 5 water molecules per Å^2. This value is relatively high, especially considering the literature [31] that had calculated a value of about few molecules for Å^2 absorbed for the formation of a water monolayer on a calcite surface. It is reasonable to assume that in our case a multilayer, is present at the grain-air interface. Sample W15 shows higher value of N_H/S_{Q_2}, and this can be due to the higher amount of salt, which has a higher affinity towards water.

Finally, a rough estimation of the average size r of "big" mesoscopic units (voids/mineral aggregates) was attempted. Considering each sample formed by n spherical grains of total volume V_t and total surface area S_t, knowing the apparent density ρ_{app} and the bulk density ρ_{bulk} of limestones and corresponding bulk materials, respectively, the ratio V_t/S_t provides the average radius of the grains:

$$\frac{V_t}{S_t} = \frac{\frac{4}{3}n\pi r^3}{4n\pi r^2} = \frac{r}{3} = \frac{1 - \frac{\rho_{app}}{\rho_{bulk}}}{S_{Q_1}} \tag{13}$$

where the total area of the interface S_t is in this case evaluated with the gauge $1/Q_1$.

Table 4 Backbone D_B and percolation D_P fractal dimensions for all the investigated samples (see text for details)

Sample	D_B	D_P
U	2.74	2.98
W1	2.69	2.99
W6	2.68	2.98
W15	2.62	3.00
W1-nLime	2.62	2.98
W6-nLime	2.64	2.98
W15-nLime	2.46	2.99

Error bars for D_B and D_P are of the order of 1 %

Table 5 Prefactor C_2, contrast K^2, total area of the interfaces per unit volume S_{Q_1} and S_{Q_2}, number of hydrogen atoms per unit interface area N_H/S_{Q_2}, average pore radius r as extracted from SANS data

Sample	C_2 ($\times 10^{-6}$)	K^2 (10^{20} cm^{-4})	S_{Q_1} (m^2/cm^3)	S_{Q_2} (m^2/cm^3)	N_H/S_{Q_2} (10^{17} cm^{-2})	r (µm)	r_{Hg} (µm)
U	6.9	16.85	1.18	1.92	0.98	0.46	0.52
W1	8.7	16.85	1.59	2.54	1.17	0.51	0.57
W6	7.1	16.85	1.63	2.43	0.97	0.57	0.59
W15	5.1	16.85	1.03	1.60	1.47	0.82	0.40
W1-nLime	4.1	16.85	0.58	1.00	1.26	1.15	0.55
W6-nLime	7.3	16.85	1.47	2.28	0.96	0.62	0.63
W15-nLime	3.4	16.85	1.04	1.43	0.99	0.84	0.82

The overall systematic accuracy is of the order of 10 % for C_2, S_{Q_1} and S_{Q_2}, and 1 % for r. K^2 values are very accurate, being obtained from a calculation made from the chemical composition, which is known with accuracy. The number of hydrogen atoms per unit interface area N_H/S_{Q_2}, and the average pore radius r_{Hg} (extracted from Hg intrusion porosimetry) are also reported

The so calculated r values are also summarized in Table 5. It is worth of note that r turns out to increase as a consequence of consolidation, occurrence that evidences once again the consolidating efficiency of nanolime. Furthermore, these values have been compared with the average pore radius obtained, for the studied limestones, by usual porosimetric analysis using Hg as filling agent [11]. An overall agreement of the data obtained by Hg porosimetry with those extracted from neutron scattering data can be recognized. This agreement, already observed in other materials of historical–artistic interest [13], confirms once again the appropriateness of the parameter α in investigating, in a noninvasive or at least microdestructive way, porosity. Some discrepancies are revealed for W15 and W1-nLime samples, but they can be mainly ascribed to the fact that, in contrast to Hg porosimetry by which only open pores are accessible, SANS explores both open and closed porosity. Furthermore, if, on the one side, r_{Hg} is directly extracted by MIP, r, on the other side, is an indirect result based on the calculation performed according to Eq. (13), so taking into account all the assumptions involved. Again, mercury porosimetry probes only pores with size larger than 50 Å, whereas r obtained in our model starts from the fractal exponent α, and, hence, will be associated to "big" units (voids/mineral aggregates) whose size falls out of the experimental window (i.e. $\geq 1/Q_{min} \sim 260$ Å). In addition, we remark that, among "big" units, there is no possibility to distinguish between grain and voids. Finally, in the calculation of r, we used spherical grains, whereas Hg injection porosimetry probes pores cylindrical in shape.

4 Conclusion

In the present paper, a fractal model has been used to analyse SANS patterns of Modica stones, a limestone largely used in the Baroque architecture of eastern Sicily. It

has been explored the evolution of the stone microstructure during salt crystallization weathering, as well as after treatment with nanolime, an innovative consolidating agent used in the field of restoration.

The comparison between the radius on gyration (R_g) measured for untreated and weathered stones suggested the formation of smaller mesoscopic structures, which can be associated to the new porosity generated by cracks, but also to the salt crystals within the pores. Such crystals tend to grow with weathering cycles, as testified by the increasing of R_g. Again, weathering is shown to give rise to an enhancement of the sharpness of the interfaces, as expressed by the increased value of α. On the other side, the consolidation induces the formation of bigger aggregates and the reduction of the sharpness of the interfaces, representing an evidence of the consolidating efficiency.

The number of hydrogen atoms on the grain-air interface has been calculated for all samples. H-atoms are related to the presence of water, about 5 water molecule per Å^2 have been estimated, this is compatible with a multi-layered water on the interface. Moreover, the higher amount of hydrogen on weathered samples can be associated with the presence of sodium sulphate within the stone porosity, since this salt has strong hygroscopic behaviour. SANS technique has shown a good sensitivity for probing differences of the microstructures in stone materials induced by salt weathering, as well as by consolidation treatments, that can be hardly checked with common analytical techniques. Finally, the advantages of SANS in detailed studies of particle/pore distributions, with respect to routine determination of porosity, have been discussed, and the obtained results can give a relevant contribution in the restoration procedure of historic–artistic monuments, that is not possible without a full understanding of textural and physical–mechanical properties of the involved materials.

References

1. B.O. Fobe, G.J. Vleugels, E.J. Roekens, R.E. Van Grieken, B. Hermosin, J.J. Ortega-Calvo, A.S. Del Junco, C. Saiz-Jimenez, Environ. Sci. Technol. **29**, 1691 (1995)
2. D. Camuffo, M. Del Monte, C. Sabbioni, O. Vittori, Atmos. Environ. **16**, 2253 (1982)
3. G. Barbera, G. Barone, V. Crupi, F. Longo, G. Maisano, D. Majolino, P. Mazzoleni, S. Raneri, J. Teixeira, V. Venuti, Eur. J. Mineral. **26**, 189 (2014)
4. R. Giordano, J. Teixeira, M. Triscari, U. Wanderlingh, Eur. J. Mineral. **19**, 223 (2007)
5. R. Coppola, A. Lapp, M. Magnani, M. Valli, Appl. Phys. A Matter Sci. Process. **74**, s1066 (2002)
6. M.F. La Russa, S.A. Ruffolo, C.M. Belfiore, P. Aloise, L. Randazzo, N. Rovella, A. Pezzino, G. Montana, Period Mineral. **82**, 113 (2013)
7. M. Koniorczyk, D. Gawin, Constr. Build. Mater. **36**, 860 (2012)
8. D. Chelazzi, G. Poggi, Y. Jaidar, N. Toccafondi, R. Giorgi, P. Baglioni, J. Colloid Interface Sci. **392**, 42 (2013)
9. S.A. Ruffolo, M.F. La Russa, P. Aloise, C.M. Belfiore, A. Macchia, A. Pezzino, G.M. Crisci, Appl. Phys. A **114**, 753 (2013)
10. M.F. La Russa, A. Macchia, S.A. Ruffolo, F. De Leo, M. Barberio, P. Barone, G.M. Crisci, C. Urzì, Int. Biodeterior. Biodegrad. **96**, 87 (2014)
11. S.A. Ruffolo, M.F. La Russa, M. Ricca, C.M. Belfiore, A. Macchia, V. Comite, A. Pezzino, G.M. Crisci, Bull. Eng. Geol. Environ. (2015). doi:10.1007/s10064-015-0782-1
12. J. Teixeira, J. Appl. Crystallogr. **21**, 781 (1988)
13. G. Barone, V. Crupi, D. Majolino, P. Mazzoleni, J. Teixeira, V. Venuti, J. Appl. Phys. **106**, 054904/1 (2009)
14. G. Barbera, G. Barone, V. Crupi, F. Longo, G. Maisano, D. Majolino, P. Mazzoleni, J. Teixeira, V. Venuti, J. Archaeol. Sci. **40**, 983 (2013)
15. G. Barbera, G. Barone, V. Crupi, F. Longo, G. Maisano, D. Majolino, P. Mazzoleni, S. Raneri, J. Teixeira, V. Venuti, Eur. J. Mineral. **26**, 189 (2014)
16. A.P. Radlinski, E.Z. Radlinska, M. Agamalian, G.D. Wignall, P. Lindner, O.G. Randl, J. Appl. Crystallogr. **33**, 860 (2000)
17. M.F. La Russa, G. Barone, P. Mazzoleni, A. Pezzino, V. Crupi, D. Majolino, Appl. Phys. A **92**, 185 (2008)
18. C.M. Belfiore, M.F. La Russa, A. Pezzino, E. Campani, A. Casoli, Appl. Phys. A **100**, 835 (2010)
19. R.J. Dunham, in *Classification of Carbonate Rocks According to Depositional Texture*, ed. by W.D. Ham (American Association of Petroleum Geologist Memoir, Tulsa, 1962), p. 108
20. EN 12370, *Natural Stone Test Methods—Determination of Resistance to Salt Crystallization* (European Committee for Standardization (CEN), Brussels, 2001), p. 108
21. J.S. Higgins, H.C. Benoît, *Polymer and Neutron Scattering* (Clarendon, Oxford, 1994)
22. A. Guinier, G. Fournet, *Small-Angle Scattering of X-rays* (Wiley, New York, 1955)
23. G. Lucido, R. Triolo, E. Caponetti, Phys. Rev. B **38**, 9031 (1988)
24. http://www-llb.cea.fr/spectros/spectro/g5-4.html
25. R.F. Angulo, V. Alvarado, H. Gonzalez, *Fractal Dimensions from Mercury Intrusion Capillary Tests* (II LAPEC, Caracas, 1992)
26. AA VV, *Raccomandazione Normal 4/80: Distribuzione del volume dei pori in funzione del loro diametro* (CNR-ICR, Roma, 1980)
27. G. Beaucage, J. Appl. Crystallogr. **28**, 717 (1995)
28. G. Barone, V. Crupi, D. Majolino, P. Mazzoleni, J. Teixeira, V. Venuti, A. Scandurra, Appl. Clay Sci. **54**, 40 (2011)
29. A. Botti, M.A. Ricci, G. De Rossi, W. Kockelmann, A. Sodo, J. Archaeol. Sci. **33**, 307 (2008)
30. G. Barone, V. Crupi, F. Longo, D. Majolino, P. Mazzoleni, S. Raneri, J. Teixeira, V. Venuti, J. Inst. **9**, C05024/1 (2014)
31. A. Rahaman, V.H. Grassian, C.J. Margulis, J. Phys. Chem. C **112**, 2109 (2008)